This is a final manuscript of https://doi.org/10.1007/978-3-030-24568-9_20.
T. Kubota, K. Aonashi, T. Ushio, S. Shige, Y. N. Takayabu, M. Kachi, Y. Arai, T. Tashima, T. Masaki, N. Kawamoto, T. Mega, M. K. Yamamoto, A. Hamada, M. Yamaji, G. Liu and R. Oki, 2020: Global Satellite Mapping of Precipitation (GSMaP) Products in the GPM Era, In: Levizzani V., Kidd C., Kirschbaum D., Kummerow C., Nakamura K., Turk F. (eds) Satellite Precipitation Measurement. Advances in Global Change Research, vol 67., Springer, Cham.

The original source of publication can be accessible through
https://doi.org/10.1007/978-3-030-24568-9_20

Chapter 20
Global Satellite Mapping of Precipitation (GSMaP) Products in the GPM Era

Takuji Kubota[1], Kazumasa Aonashi[2], Tomoo Ushio[3], Shoichi Shige[4], Yukari N. Takayabu[5], Misako Kachi[1], Yoriko Arai[6], Tomoko Tashima[1], Takeshi Masaki[6], Nozomi Kawamoto[6], Tomoaki Mega[3], Munehisa K. Yamamoto[4], Atsushi Hamada[7], Moeka Yamaji[1], Guosheng Liu[8] and Riko Oki[1]

[1] Earth Observation Research Center, Japan Aerospace Exploration Agency, Ibaraki, Japan.
[2] Meteorological Research Institute, Japan Meteorological Agency, Ibaraki, Japan.
[3] Tokyo Metropolitan University, Tokyo, Japan.
[4] Kyoto University, Kyoto, Japan.
[5] University of Tokyo, Chiba, Japan.
[6] Remote Sensing Technology Center of Japan, Tokyo, Japan.
[7] University of Toyama, Toyama, Japan.
[8] Florida State University, FL, USA.

Abstract As the Japanese Global Precipitation Measurement (GPM) product, the Global Satellite Mapping of Precipitation (GSMaP) has been provided by the Japan Aerospace Exploration Agency (JAXA) to distribute hourly global precipitation map with 0.1 × 0.1 deg lat/lon grid. Since JAXA started near-real-time processing of the GSMaP on November 2007, there have been various significant progresses of the GSMaP. This paper summarizes GSMaP products and related algorithms in the GPM era and shows validation results in Japan and United States.

20.1 Introduction

Satellite-based precipitation datasets have been developed to achieve higher spatial and temporal resolutions using combined data from passive microwave (PMW) sensors in low Earth orbit and infrared (IR) radiometers in geostationary Earth orbit. Global Satellite Mapping of Precipitation (GSMaP) is a blended PMW–IR precipitation product and has been developed in Japan for the Global Precipitation Measurement (GPM) mission (Hou et al. 2014; Skofronick-Jackson et al. 2017) as the Japanese GPM standard product.

The GSMaP algorithms have been improved based on various attributes derived from the Tropical Rainfall Measuring Mission (TRMM) precipitation radar (PR), which was the first spaceborne precipitation radar and operated during 1997–2015 (Kummerow et al. 1998; Kozu et al. 2001). The combined use of PR and the TRMM microwave imager (TMI) has greatly improved rainfall estimation technique. Furthermore, the GPM Core Observatory was launched in Feb. 2014, carrying the Dual-frequency Precipitation Radar (DPR) and the GPM Microwave Imager (GMI). The DPR

and the GMI have advanced this by expanding the coverage of observations to higher latitudes than those obtained by the TRMM. Moreover, precipitation information based on differential scattering properties of the dual frequencies by the DPR can be helpful for improving the PMW algorithms.
The GSMaP project was initiated and sponsored by the Japan Science and Technology Agency under the Core Research for Evolutional Science and Technology from November 2002 (Okamoto et al. 2005; Kubota et al. 2007), and its major activity was completed in March 2008. Since April 2008, GSMaP activities have been implemented under the JAXA Precipitation Measuring Mission (PMM) Science Team. Since JAXA started near-real-time processing of the GSMaP on November 2007 (Kachi et al. 2011), there have been various significant progresses of the GSMaP in the GPM era. This paper summarizes the recent progress of the GSMaP products and related algorithms. Section 2.2.3.2 provides an overview of the GPM-era GSMaP products. Section 2.2.3.3 describes recent GSMaP algorithms. Section 2.2.3.4 illustrates validation results in Japan and United States. Conclusions are given in Section 2.2.3.5.

20.2 GSMaP product list in the GPM era

The GSMaP products in the GPM era mainly comprise “standard product,” “near-real-time product,” “real-time product”, and “reanalysis product”. Table 1 shows the GSMaP product list in the GPM era. The horizontal resolution is 0.1 × 0.1 deg lat/lon grid, and the temporal resolution is 1 hour. All products are accessible through the “JAXA Global Rainfall Watch” website (http://sharaku.eorc.jaxa.jp/GSMaP/) (see Fig. 1). In addition, the standard products and the near-real-time products are also accessible via the JAXA Globe-Portal (G-Portal) (https://www.gportal.jaxa.jp).
The standard products are processed three days after observations and consist of satellite-only hourly precipitation rate (GSMaP_MVK, hereafter, MVK) and gauge-adjusted hourly precipitation rate (GSMaP_Gauge, hereafter, GA).
On the other hand, the near-real-time products are processed 4 hours after observations and consist of satellite-only hourly precipitation rate (GSMaP_NRT, hereafter, NRT) and gauge-adjusted hourly precipitation rate (GSMaP_Gauge_NRT, hereafter, GA_NRT).

Table 1. GSMaP product list in the GPM era

<table>
<tr><th>Product name</th><th>Variables</th><th>Resolution</th><th>Latency</th><th>Update interval</th></tr>
<tr><td rowspan="2">Standard product</td><td>Hourly Precip Rate (GSMaP_MVK)</td><td rowspan="7">Horizontal:

0.1 × 0.1 deg lat/lon

Temporal:

1 hour</td><td rowspan="2">3 days</td><td rowspan="4">1 hour</td></tr>
<tr><td>Gauge-adjusted Hourly Precip Rate (GSMaP_Gauge)</td></tr>
<tr><td rowspan="2">Near-real-time product</td><td>Hourly Precip Rate (GSMaP_NRT)</td><td rowspan="2">4 hours</td></tr>
<tr><td>Gauge-adjusted Hourly Precip Rate (GSMaP_Gauge_NRT)</td></tr>
<tr><td>Real-time product</td><td>Hourly Precip Rate (GSMaP_NOW)</td><td>0 hours</td><td>0.5 hour</td></tr>
<tr><td rowspan="2">Reanalysis product</td><td>Hourly Precip Rate (GSMaP_RNL)</td><td colspan="2" rowspan="2">occasionally reprocesses past periods data</td></tr>
<tr><td>Gauge-adjusted Hourly Precip Rate (GSMaP_Gauge_RNL)</td></tr>
</table>

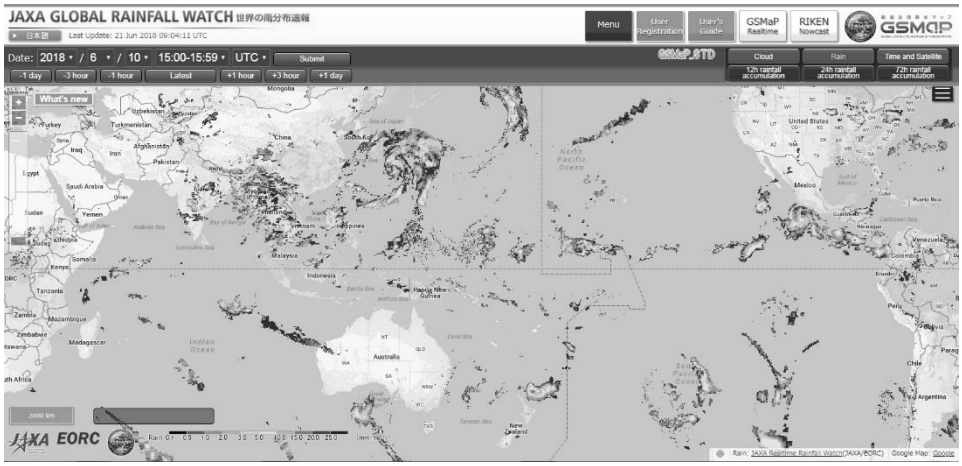

Figure 1. Image of "JAXA Global Rainfall Watch" website (http://sharaku.eorc.jaxa.jp/GSMaP/)

The near-real-time algorithm is based on the standard algorithm, but some simplifications in the processing are implemented to keep operability and data latency in near-real-time. The major differences between the near-real-time and standard processing are as follows.

- In the near-real-time processing, forecast data are used as atmospheric information.
- Latest available data are used as sea surface temperature (SST) information.
- Only temporarily forward cloud movement is used in the PMW–IR combined algorithm.
- Only statistical parameters are used in gauge-adjustment algorithm

Furthermore, the real-time product "GSMaP_NOW" (hereafter, NOW) is processed to produce estimates at the current hour. The NOW has been provided over the Japan Meteorological Agency (JMA)'s geostationary satellite "Himawari-8" (Bessho et al. 2016) region since November 2015. Since November 2018, the NOW has been extended to regions of the European Organization for the Exploitation of Meteorological Satellites (EUMETSAT). Further extensions to other global domains were established using satellite data from the National Oceanic and Atmospheric Administration (NOAA) in June 2019. Major differences between real-time and near-real-time processing are as follows.

- In the real-time processing, data that is available within 0.5 hour after observations are collected, while the data that is available within 3 hours are collected in the near-real-time processing.
- Data received at direct readout stations for Advanced Microwave Scanning Radiometer-2 (AMSR2) and the Direct Broadcast Network (DBNet) are used to increase PMW data collection in the real-time processing.
- A 0.5-hour forward extrapolation (future direction) applied by cloud motion vector is used to produce estimates at the current hour.
- The NOW product is updated half-hourly, while other products are updated hourly.

These features and differences of the products are directly related to accuracies of the products, which are later verified in this paper using gauge-corrected ground-radar dataset.
Reanalysis products (GSMaP_RNL and GSMaP_RNL_Gauge) are calculated with Japanese 55-year reanalysis (JRA55) (Kobayashi et al. 2015; Harada et al. 2016) and occasionally reprocesses past periods data. The data of March 2000 to February 2014 are now available in the reanalysis product. Our preliminary analyses show differences between the reanalysis and the standard

products are little and therefore, users can combine these for long-term analyses. This reanalysis product has been scheduled to be integrated into the standard product around early 2020 in the JAXA GPM mission.
In addition, the RIKEN, a research institute in Japan, has provided GSMaP RIKEN Nowcast (GSMaP_RNC) data developed based upon Otsuka et al. (2016) since 2017. This data is also available from JAXA/EORC ftp site.

20.3 Algorithm Descriptions

The GSMaP products were majorly updated on September 2014 and January 2017 after the GPM Core Observatory was launched. The product corresponding to the algorithm updates on September 2014 is referred to as Product version V03 and Algorithm version V6, and the product corresponding to the algorithm updates on January 2017 is referred to as Product version V04 and Algorithm version V7. In this section, algorithms are summarized referring to previous papers, and algorithm versions are used for classification between both updates. Evolutions of the algorithms from V6 to V7 are briefly summarized in Section 2.2.3.3.9. Currently, both V6 and V7 algorithms are together processed in the JAXA.

20.3.1 Overall algorithm framework

Core algorithms of the GSMaP products are based on those provided by the GSMaP project: PMW precipitation retrieval algorithm, PMW–IR combined algorithm, and gauge-adjustment algorithm. Figure 2 shows a process flowchart for the GSMaP product.
The GSMaP algorithms use several ancillary data as operational inputs. JMA global analysis (GANAL) and forecast (FCST) data set, which are 6-hourly data with 0.5 degree grid box, are used as ancillary data of atmospheric conditions to calculate look-up tables (LUTs), which are referred by the PMW algorithms. GANAL data are used to process standard products, and FCST data are used to process near-real-time products. In the reanalysis product, the JRA-55 data (6-hourly, TL319L60 model grid) are used instead of operational data.
The JMA merged satellite and in situ data global daily SST (MGDSST) data, which is on a 0.25 degree grid box, are used as ancillary data of SST for calculating LUTs, which are referred by the PMW algorithms.
The NOAA Climate Prediction Center (CPC) unified gauge-based analysis of global daily precipitation (Chen et al. 2008), which is on a 0.5 degree grid box, has been used as an input to calculate gauge-adjusted rainfall.
Climatological sea ice values from the JAXA Advanced Microwave Scanning Radiometer for EOS (AMSR-E) product were used for screening sea ices in V6, while ancillary data for surface snow were not used. In the V7, the NOAA National Environmental Satellite, Data, and Information Service (NESDIS) multi-sensor snow/ice cover maps were used as ancillary data to detect the sea ice and the surface snow, which are referred by the PMW algorithms.

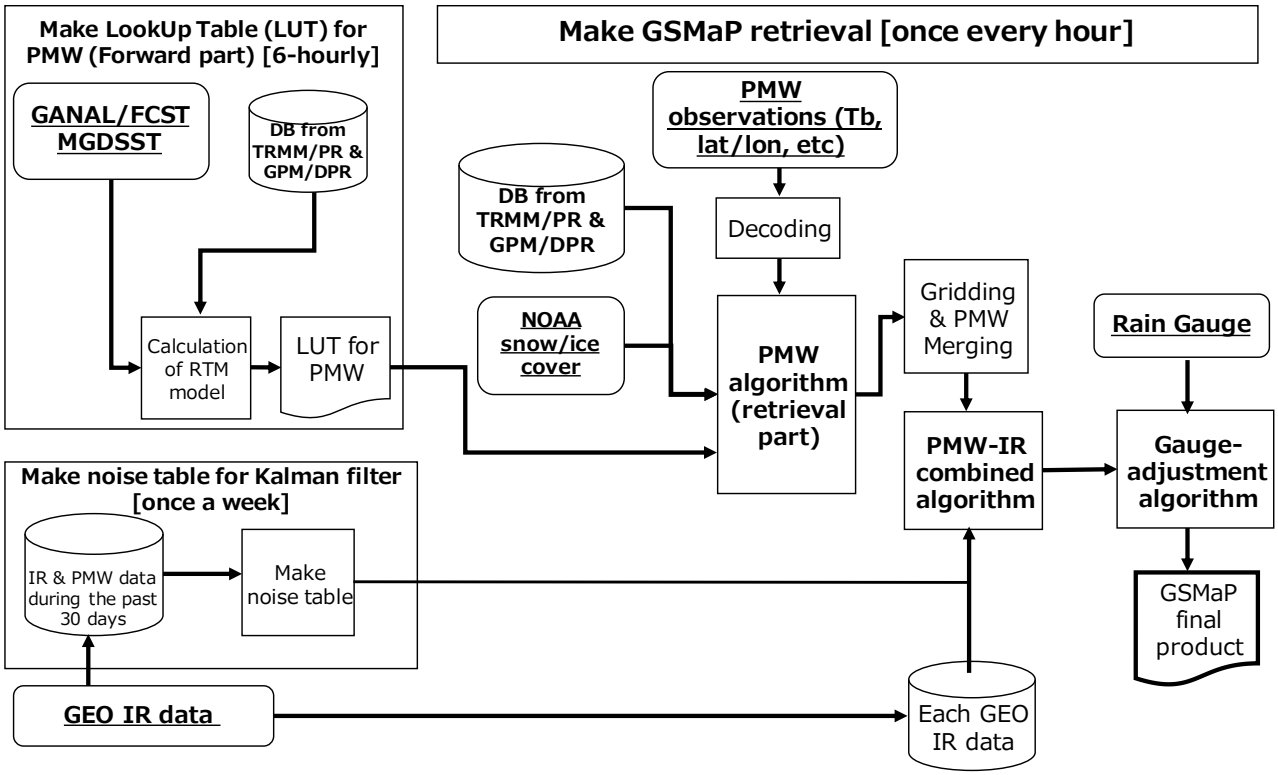

Figure 2. Process flowchart for the GSMaP product

20.3.2 Outline of the PMW algorithm

The PMW algorithm retrieves global precipitation rates from brightness temperatures (Tbs) of the PMW sensor. The PMW algorithm has been improved based upon the Microwave Imager (MWI) algorithm of Aonashi et al. (2009). The basic idea of the PMW algorithm is to find precipitation rates that give radiative transfer model (RTM)-calculated Tbs that best fit with the observed Tbs. The MWI algorithm employs polarization corrected temperatures (PCTs) at higher frequencies (37 and 85 GHz for the TMI) over land and coast, and Tbs with vertical polarization at lower frequencies (10, 19, and 37 GHz for the TMI) in addition to the higher frequency PCTs over ocean. Several modifications due to sensor specifications are highlighted in Section 2.2.3.3.5.

20.3.3 Methodology in the PMW algorithm

The PMW algorithm consists of a forward calculation part and a retrieval part. In the forward calculation part, LUTs are calculated for homogeneous precipitation by incorporating atmospheric and surface variables of the GANAL or FCST data and precipitation physical models based on spaceborne precipitation radar observations into the RTM program of Liu (1998). The precipitation physical models have been developed by previous works (Takayabu 2008; Takahashi and Awaka 2005; Kozu et al. 2009; Yamaji et al. 2017). In construction of the model, the TRMM/PR data were used in V6 algorithm, and both the TRMM/PR and GPM/DPR data were used in the V7 algorithm. The land surface emissivity was used from the TRMM observations (Furuzawa et al. 2012). LUTs for inhomogeneous precipitation are derived from the above LUTs using the approximations of Aonashi and Liu (2000) and Kubota et al. (2009a).
The retrieval part of the PMW algorithm performs a detection of rainfall, a retrieval using scattering signals, and an over-ocean retrieval using emission signals. Methods of Seto et al. (2005, 2008, 2016), Mega and Shige (2016), and Kida et al. (2009, 2010a) were adopted for the rainfall detection over land, coastal areas, and ocean, respectively. Seto et al. (2005) was used in both V6 and the V7

in the TMI over-land algorithm. In the algorithms for the other PMW sensors, Seto et al (2008) was applied in the V6, and a method using the DPR and the GMI (Seto et al. 2016), similar to Seto et al. (2005) of the TRMM, was applied in V7. In addition, the over-ocean detection is improved in V7 by consideration of cloud liquid water estimated at Tbs at 37GHz (Aonashi et al. 2016).
Dual-frequency PCTs (at 37 and 85 GHz for TMI) are employed in retrievals using scattering signals. An adjustment method is introduced using indices of frozen precipitation depth and surface temperature. In the over-ocean retrieval using emission signals, a rainfall rate is derived by minimizing a cost function for lower frequency, vertically polarized Tbs (10, 19, and 37 GHz for the TMI), with the scattering retrievals as the first guess.

20.3.4 Orographic/non-orographic rainfall classification scheme

Over coastal mountain ranges, heavy rainfall can be caused by shallow orographic rainfall, which is inconsistent with the assumption in the PMW algorithm that heavy rainfall results from deep clouds with significant ice. For example, severe underestimations of the GSMaP rainfall estimates in old versions were found over orographic rainfall areas in Japan (Kubota et al. 2009b). Therefore, orographic/non-orographic rainfall classification scheme was developed (Shige et al. 2013; Taniguchi et al. 2013) and installed in the PMW algorithm. LUTs for orographic rainfall are calculated according to Shige et al. (2014). In addition, detection schemes have been developed for orographic rainfall areas where the LUTs for orographic rainfall are applied. The scheme and modified one were installed in V6 (Yamamoto and Shige 2015) for the TMI and V7 (Yamamoto et al. 2017) for all sensors, respectively.

20.3.5 Modifications due to sensor specifications

While the basic structure described above is common in the PMW algorithms, several modifications have been applied because of sensor specifications. Shige et al. (2009) developed a Microwave Sounder (MWS) algorithm which combines an emission-based estimate from Tb data at 23 GHz and a scattering-based estimate from Tb data at 89 GHz over ocean, depending on a scattering index computed from Tb at both 89 and 150 GHz. The scattering index, which is designed on the basis that Tb decreases in response to scattering by precipitation at these frequencies, also responds to emission in light rain with a low concentration of cloud liquid water, leading to detection of light rain pixel (Kida et al. 2010b). In addition, the MWS algorithm adopts a rain/no-rain classification method over land using 150 GHz and 183 GHz channels, as described in Kida et al. (2017).
The Special Sensor Microwave Imager/Sounder (SSMIS) does not have 10 GHz channels, as well as the Special Sensor Microwave/Imager (SSM/I). Therefore, the over-ocean algorithms for the SSMIS and the SSM/I calculate estimates from normalized polarization differences (Petty 1994) at 19 GHz, and combine them with emission-based estimates from Tb at 19 GHz vertical polarization and scattering-based estimates from the PCTs at 89 GHz (Hashizume et al. 2006; Kubota et al. 2011).

20.3.6 Snowfall estimation method

Recently, a snowfall estimation was implemented in the V7 algorithm (Kubota et al. 2018). In the V6 or earlier versions, there was no snowfall estimation in the GSMaP products. The snowfall estimation method can be divided into a method of classifying precipitation phase (rain/ snow) and if determined to be snow, a method of estimating snowfall intensity. Here, the rain/snow classification method is based upon the method of Sims and Liu (2015), with inputs of the GANAL/FCST data. Based on the results of past ground observations, the method determines the precipitation phase, if rain or snow. The snowfall intensity estimation method was developed using the CloudSat-GPM coincidence dataset, based upon the method of Liu and Seo (2013). This

statistical method which uses radar observations to train the PMW data uses information contained in the first three principal components that resulted from an empirical orthogonal function. In the V7, the snowfall estimation method was installed in the GMI and the SSMIS.

20.3.7 PMW–IR combined algorithm

The PMW–IR combined algorithm integrates PMW data with infrared radiometer data to achieve high temporal (1 hour) and spatial (0.1 degree) resolution global precipitation estimates. The product is produced based on a Kalman filter model that refines the precipitation rate propagated based on the atmospheric moving vector derived from two successive IR images (Ushio et al. 2009). Noises and coefficients in the Kalman filter model are calculated once a week using IR and PMW data during the past 30 days, as described in Fig.2. As noted in Section 2.2.3.2, both temporarily forward and backward cloud motions are used in the MVK, while only temporarily forward cloud motion is used in the NRT and the NOW.

20.3.8 Gauge-adjustment algorithm

The GA algorithm adjusts the MVK estimates with the NOAA/CPC unified gauge-based analysis of global daily precipitation. The estimate is adjusted only over land. The rain rate over ocean from GA and GA_NRT are the same as those from MVK and NRT, respectively. The algorithm uses an optical estimation scheme, in which the solution is calculated by maximizing the probability density function defined in the system model (Mega et al. 2019). The hourly rain rate of the GA is adjusted by this algorithm so that the sum of the 24-hour rain of the GA rate is roughly the same as the gauge measurement. A number of gauges available in each 0.5deg lat/lon grid box was considered in V7, while it was not considered in V6. While the parameters were assumed to be constant in the V6 GA_NRT, statistical parameters were improved to be calculated from data during the past 30 days in the V7 GA_NRT. On the other hand, a method similar to the GA_NRT V7 was also applied to the GA_NRT V6 as a minor version-upgrade in December 2018. Therefore, the GA_NRT method is basically identical between V6 and V7 after Dec. 2018.

20.3.9 Brief summary of evolutions from V6 to V7

In the above subsections, the algorithms were described for both V6 and the V7. Table 2 provides a brief summary of evolutions in the algorithms from V6 to V7.

Table 2. Brief summary of evolutions in the algorithms from V6 to V7.

Item	V6	V7
Utilization of spaceborne radar data in precipitation physical models	TRMM/PR	TRMM/PR and GPM/DPR
Ancillary data for sea ice	JAXA AMSR-E (climatological)	NESDIS
Ancillary data for surface snow	None	NESDIS
Detection over the land for MWI/SSMIS/GMI	Seto et al. (2008)	Seto et al. (2016)
Detection over the ocean for MWI/SSMIS/GMI	Kida et al. (2009, 2010a)	Kida et al. (2009, 2010a), Aonashi et al. (2016)
Orographic/non-orographic rainfall classification scheme	Yamamoto and Shige (2015) for the TMI	Yamamoto et al. (2017) for all sensors
Snowfall estimation method	Not implemented	Implemented in GMI/SSMIS
Consideration of gauge numbers in the Gauge-adjustment algorithm	Not included	Included

20.4 Validation results of the GSMaP Products

The validation of satellite products using ground instruments can be helpful to understand the products strengths and limitations. Validation results using gauge-corrected radar data around Japan and the contiguous United States (CONUS) are shown in this section. The GSMaP V6 products are analyzed here, and the validation using the GSMaP V7 has been left for future works. As noted in the previous section, the GA_NRT V6 had significant improvements in Dec. 2018, and thus it is skipped in the validations.

20.4.1 Comparisons of the GSMaP products around Japan

This subsection compares the GSMaP Products listed in Section 2.2.3.2 around Japan with reference to a ground-radar dataset calibrated by rain gauges provided by the JMA, termed "Radar-AMeDAS" data. Here, observation areas of the Radar-AMeDAS were limited to within 250km of radar sites. In addition, the NOAA/NESDIS hydro-estimator (H-E) (Vicente et al., 1998, 2002; Scofield and Kuligowski 2003) is also analyzed because the H-E is a well-known IR-based satellite rainfall product with a latency of less than 30 minutes. Although previous works (e.g., Ebert et al. 1996; Smith et al. 1998; Beck et al. 2017) indicate that the IR-based products are less accurate than the PMW-based product, the earlier latency of the IR-based product can be attractive for users. The NOW system was developed with a higher priority to the latencies, and comparisons between the H-E and the NOW are interesting as the products with the earlier latencies.

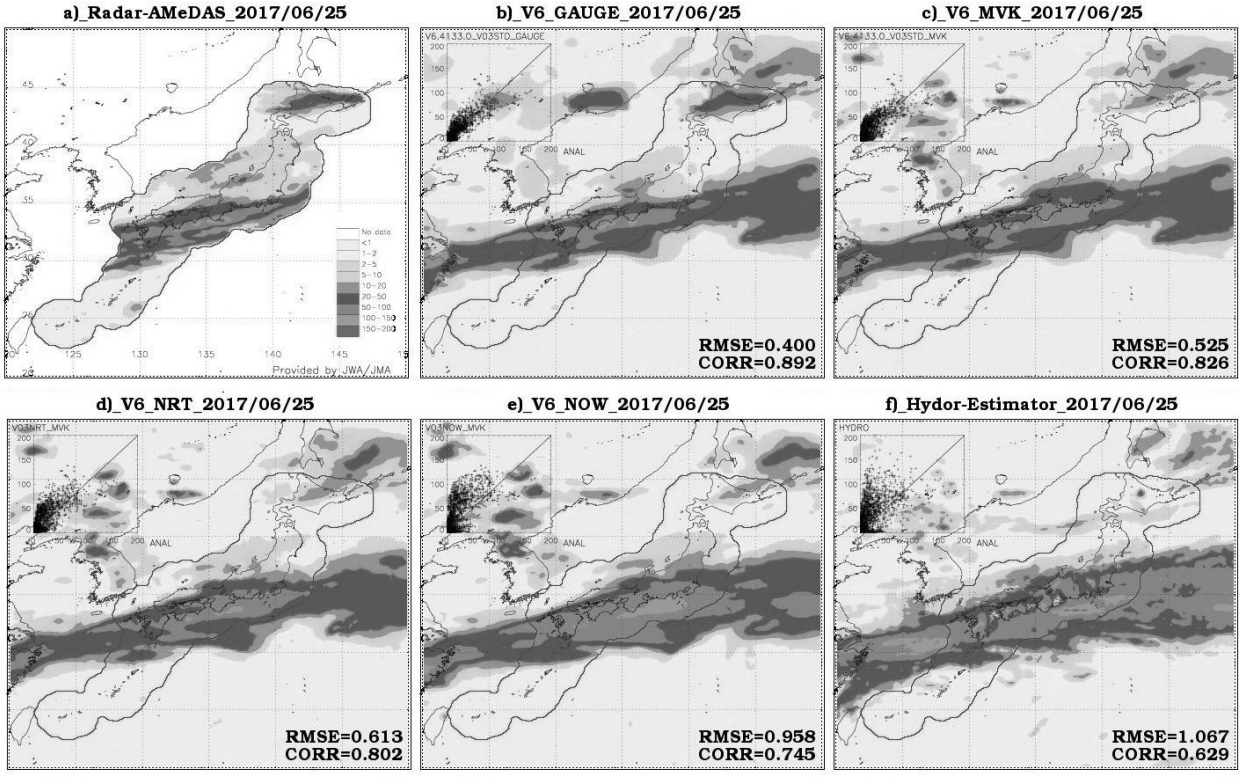

Figure 3. Distribution of the daily rain amount around Japan on June 25, 2017 for a) JMA radar-AMeDAS, b) GA V6, c) MVK V6, d) NRT V6, e) NOW V6, and f) Hydro-Estimator (H-E).

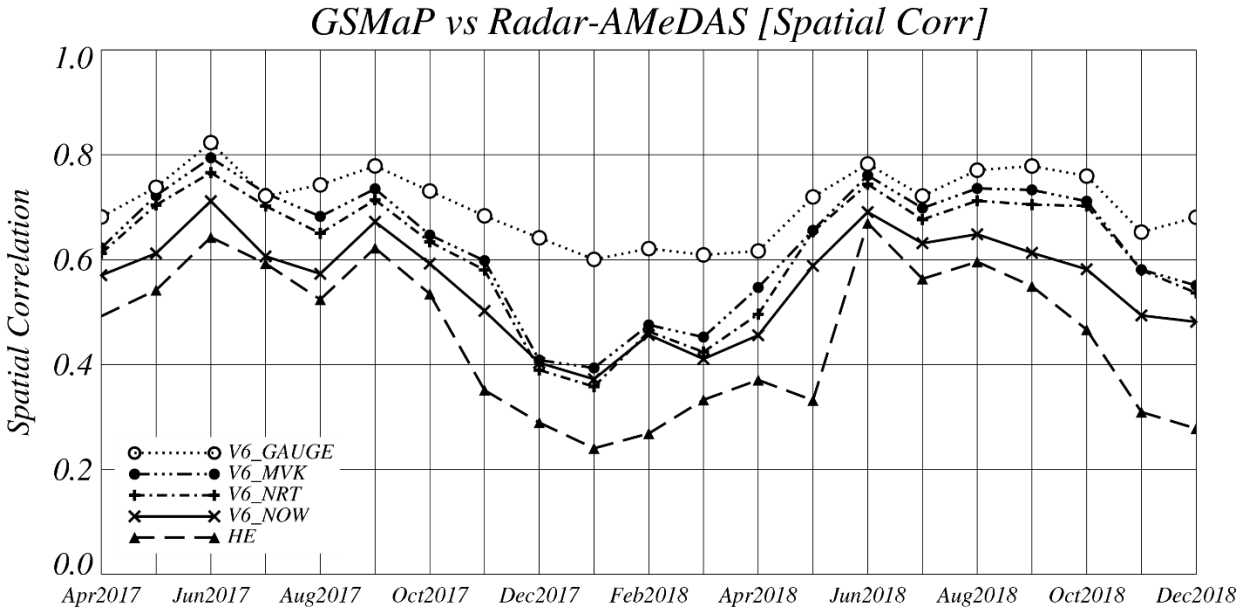

Figure 4. Time series of the correlation coefficient (CC) for the GSMaP products and the H-E with reference to the JMA's Radar-AMeDAS around Japan in 0.25 deg lat/lon grid and daily accumulation from Apr. 1, 2017 to Dec. 31, 2018. Monthly mean was applied to the daily CC values. Open circles denote the GA; closed circles denote the MVK; plusses denote the NRT; crosses denote the NOW; and triangles denote the H-E.

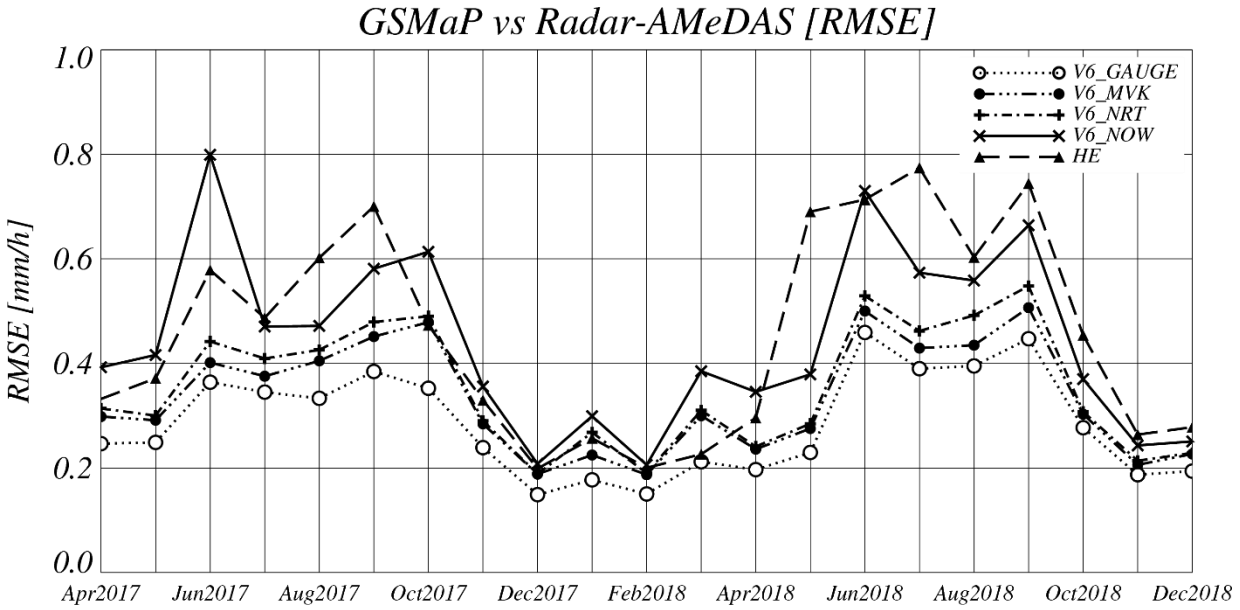

Figure 5. Time series of the root mean square error (RMSE) for the GSMaP products and the H-E with reference to the JMA's Radar-AMeDAS around Japan in 0.25 deg lat/lon grid and daily accumulation from Apr. 1, 2017 to Dec. 31, 2018. Monthly mean was applied to the daily RMSE values. Open circles denote the GA; closed circles denote the MVK; plusses denote the NRT; crosses denote the NOW; and triangles denote the H-E.

Table 3. Values of the CC and RMSE averaged during 21 months: April 2017 to December 2018.

Product name	GA	MVK	NRT	NOW	H-E
CC	0.71	0.63	0.61	0.56	0.46
RMSE (mm/h)	0.28	0.33	0.35	0.44	0.45

Figure 3 shows the horizontal distribution of the daily rain amount around Japan in 0.25 deg lat/lon grid on June 25, 2017. The rainfall pattern related to the Baiu front, which is typical in a rainy season around Japan, was around the southern coast of the Japan main islands. Here, root mean square error (RMSE) and correlation coefficient (CC) are adopted as statistical indices and noted in the figures. The CC is sensitive to the rainfall spatial pattern, and the RMSE is sensitive to the rainfall intensity. Among the GSMaP products, the GA has the lowest RMSE and highest CC, while the NOW has the highest RMSE and lowest CC. On the other hand, the NOW shows better results than the H-E for this case study.

To obtain more reliable results, these analyses were extended to a 21-month period: Apr. 1, 2017 to Dec. 31, 2018. Figure 4 shows the time series of the CC for the GSMaP products and the H-E with reference to the JMA's Radar-AMeDAS around Japan, and Figure 5 shows the time series of the RMSE. Table 3 shows the CC and RMSE averaged values over 21 months. Table 3 clearly indicates the accuracies of the GSMaP products, where GA > MVK > NRT > NOW. This tendency was stable in time series of the CC (Fig.4) and the RMSE (Fig. 5). The GA has the best accuracy because of the adjustment using the gauge. As in Kubota et al. (2009b) and Kachi et al. (2011), seasonal changes of the spatial correlation coefficients were found for the MVK, the NRT, and the NOW, because of poor skills caused by false signals related to surface snow in a cold season. On the other hand, amplitudes of the seasonal changes were smaller in the GA, and this suggests that the poor skills in the colder season were mitigated in the GA. As noted in Section 2.2.3.2, some simplifications in the processing are implemented in the NRT to keep operability and data latency in near-real-time, and thus, results of the MVK are better than those of the NRT. With comparison of the NRT and the NOW, the NOW uses the PMW–IR combined algorithm in wider areas than the NRT, due to decreases of the PMW coverages caused by its earlier data collection. As noted in Section 2.2.3.2, the NOW adopted 0.5-hour forward extrapolation. However, degradation of the 0.5-hour forward extrapolation was examined with reference to JMA's Radar-AMeDAS, and results showed that this can be regarded as small (not shown). Therefore, the poorest accuracy of the NOW may be due to the decreases of the PMW coverages. These results suggest an evident trade-off between latency and accuracy, and the choice of a GSMaP product should be dependent upon its purposes.

Considering the H-E, it has the worst CC averaged value, and its RMSE averaged is slightly worse than that of the NOW (Table 3). While the CC values for the NOW were better than those for the H-E in all periods (Figure 4), the H-E has the better RMSE values than the NOW over some periods (Figure 5). In the NOW, displacements of rain peaks can be occurred because the cloud motion may be inconsistent with the rain movement in areas of strong wind shear. Worse results of the NOW in the RMSE implies such rain peak displacements may be problematic in the NOW. Thus, the PMW-based real-time technique in the NOW showed better performances than the IR-based estimates from the H-E, in particular, for spatial patterns evaluated by the CC, while there can be still future tasks in the NOW, including issues of strong wind shear.

20.4.2 Validation using the US radar network.

This subsection provides validation results over the CONUS using Multi-Radar Multi-Sensor (MRMS) precipitation data (Zhang et al. 2011, 2016). The MRMS is a system with automated algorithms that quickly and intelligently integrates data streams from multiple radars, surface observations, and various data sources. Here, the Level-3 MRMS dataset processed in support of the GPM Mission (Kirstetter et al. 2012; Tan et al. 2016) was used. The analysis is conducted over three months: June 2015 to August 2015. The original spatial resolution of the Level-3 MRMS is 0.01 degrees, and it was converted to the same grid of 0.1 × 0.1 degrees as the GSMaP.

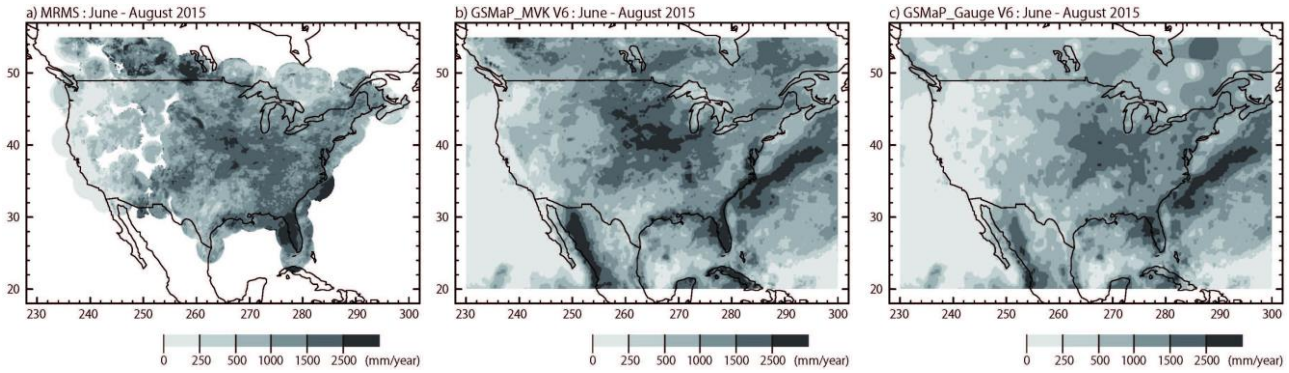

Figure 6. Accumulated rainfall (mm/yr) over three months: June to August 2015 for a) MRMS, b) MVK V6, and c) GA V6. The MRMS was analyzed over areas where the RQI was more than 50.

Figures 6 show distributions of rainfall over June to August 2015 (92 days) for the MRMS, MVK V6, and GA V6. In this paper, the MRMS was analyzed over areas where the radar quality index (RQI) was more than 50. The RQI ranges between from 0 (lowest confidence) to 100 (highest confidence) and observations of the MRMS over Rocky Mountains were partly excluded by the condition of the RQI > 50. In all the figures, rainfall is larger from the central part to the eastern part and less on the western part.

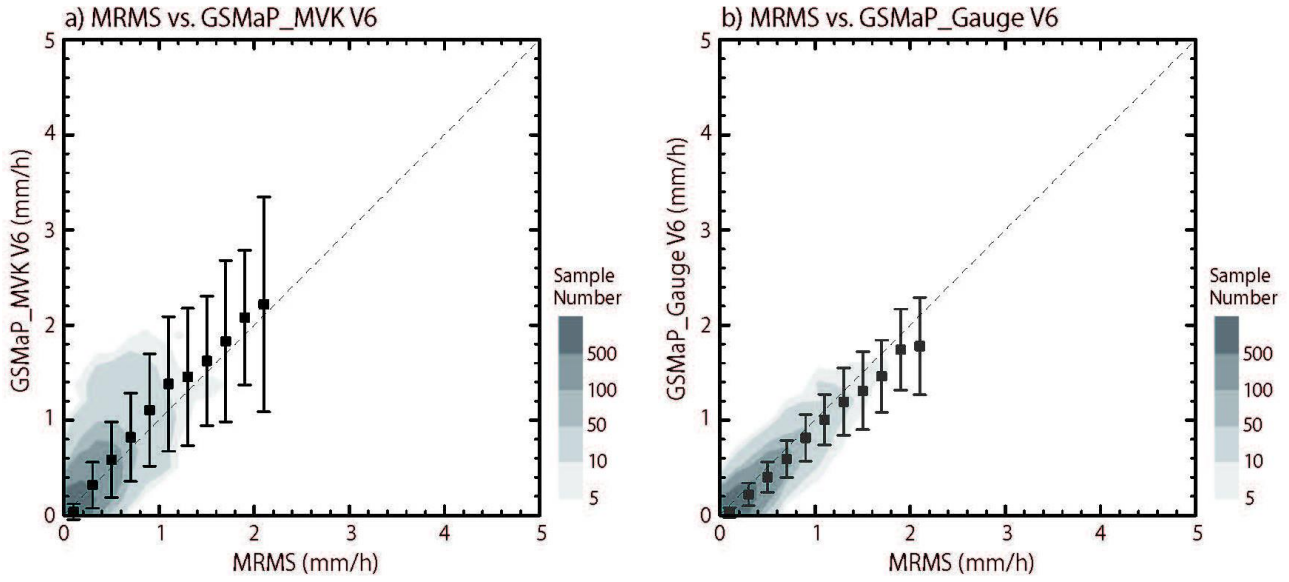

Figure 7. Two-dimensional distribution function of daily precipitation over three months from June to August 2015. Horizontal axis shows the rain rate of the MRMS, and vertical axis shows rain rates of a) MVK and b) GA. Hatch color shows the sample number of occurrences. The average value (squares) and the standard deviation (1 sigma, bars) are shown for bins of 0.2 mm/h of the MRMS with the horizontal axis as a reference. The broken line is a one-to-one line.

Two-dimensional distribution functions between the MRMS and the GSMaP are shown in Figs. 7. Here, daily rain amounts of the MRMS and the GSMaP were calculated with 379 boxes of the 1.5 × 1.5 deg lat/lon grids over the CONUS, and Figs. 7 show that both GSMaP estimates corresponded well with that of the MRMS. The statistical values denoted in Fig. 7 were calculated for every 0.2 mm/h bins of the MRMS up to 2.0–2.2 mm/h with more than 10 samples. For the MVK and GA, the averages are basically distributed along the one-to-one line, which suggests biases in both GSMaP products are relatively small. Here, errors were calculated as normalized absolute differences, i.e., |GSMaP-MRMS|/MRMS (%), in the bins. The largest value among the

error for the MVK is 26.59%, found in the bin of 1.0–1.2 mm/h, and that for the GA is 22.75% found in the bin of 0.2–0.4 mm/h. On the other hand, standard deviations of the GSMaP in bins of the MRMS, denoted by the bars, were much larger in the MVK than in the GA. The largest value among the standard deviations for the MVK is 1.13 mm/h, and that for the GA is 0.51 mm/h, found in the bin of 2.0–2.2 mm/h. This suggests that the adjustment using the gauge data largely reduced the daily variation of the errors.

20.5 Conclusions

As the Japanese GPM product, the GSMaP products have been provided by JAXA to distribute hourly global precipitation map with 0.1 × 0.1 deg lat/lon grid. Since JAXA started near-real-time processing of the GSMaP on November 2007, there have been various significant progresses of the GSMaP. This paper describes the GSMaP products and related algorithms in the GPM era. It also indicates validation results in Japan and CONUS. Based upon the validation results around Japan, the accuracy of the GSMaP products have been verified to be as follows: GA > MVK > NRT > NOW. This suggests the evident trade-off between latency and accuracy, and the choice of a GSMaP product should depend upon its purposes. The comparison between the NOW and the H-E showed that the PMW-based real-time technique in the NOW can be better than the IR-based estimates, in particular, for the spatial patterns. The validation results over the CONUS during Jun.-Aug. 2015 suggest that the adjustment using the gauge data largely reduced the daily variation of the errors.

The Algorithm version V6 released on September 2014 and Algorithm version V7 released on January 2017 after the launch of the GPM Core Observatory were described in this paper. The following version, V8 is now scheduled to be released on January 2020. Currently, algorithm developments toward V8 are in progress, which will be described in future works.

Acknowledgment

The authors would like to thank members of the JAXA PMM Science Team for their valuable contributions. The authors would like to thank Mrs. T. Higashiuwatoko and S. Ohwada of RESTEC for helpful computing assistance. The dataset of the DBNet was provided by the JMA. The dataset of the Level-3 MRMS was provided by the NASA Ground Validation team. The dataset of the Hydro-Estimator was provided by the NOAA/NESDIS.

References

Aonashi, K., and G. Liu, 2000: Passive microwave precipitation retrievals using TMI during the Baiu period of 1998. Part I: Algorithm description and validation. *J. Appl. Meteor.*, 39, 2024-2037.

Aonashi, K., J. Awaka, M. Hirose, T. Kozu, T. Kubota, G. Liu, S. Shige, S., Kida, S. Seto, N. Takahashi, and Y. N. Takayabu, 2009: GSMaP passive, microwave precipitation retrieval algorithm: Algorithm description and validation. J. Meteor. Soc. Japan, 87A, 119-136.

Aonashi, K., H. Ohwada, K. Okamoto, H. Ishimoto, M. Yamaguchi, 2016: Development of the next-generation microwave imager precipitation retrieval algorithm (No.4), *MSJ spring meeting 2016*, C154, Tokyo, Japan, May 2016 (in Japanese).

Beck, H. E., N. Vergopolan, M. Pan, V. Levizzani, A. I. J. M. van Dijk, G. P. Weedon, L. Brocca, F. Pappenberger, G. J. Huffman, and E. F. Wood, 2017: Global-scale evaluation of 22 precipitation datasets using gauge observations and hydrological modeling, *Hydrol. Earth Syst. Sci.*, 21, 6201-6217.

Bessho, K. and co-autorhos, 2016: An Introduction to Himawari-8/9— Japan's New-Generation Geostationary Meteorological Satellites, *J. Meteor. Soc. Japan*, 94, 151-183.

Chen, M., W. Shi, P. Xie, V. B. S. Silva, V E. Kousky, R. Wayne Higgins, and J. E. Janowiak, 2008: Assessing objective techniques for gauge-based analyses of global daily precipitation, *J. Geophys. Res.*, 113, D04110, doi:10.1029/2007JD009132.

Ebert, E. E., M. J. Manton, P. A. Arkin, R. J. Allam, G. E. Holpin, and A. J. Gruber, 1996: Results from the GPCP Algorithm Intercomparison Programme. *Bull. Amer. Meteor. Soc*., 77, 2875-2887.

Furuzawa, F. A, H. Masunaga, and K. Nakamura, 2012: Development of a land surface emissivity algorithm for use by microwave rain retrieval algorithms, 85231W-85231W-85212, *Proc. SPIE 8523*, Remote Sensing of the Atmosphere, Clouds, and Precipitation IV, 8523, W1-12.

Harada, Y., H. Kamahori, C. Kobayashi, H. Endo, S. Kobayashi, Y. Ota, H. Onoda, K. Onogi, K. Miyaoka, and K. Takahashi, 2016: The JRA-55 Reanalysis: Representation of atmospheric circulation and climate variability, *J. Meteor. Soc. Japan*, 94, 269-302.

Hashizume, H., T. Kubota, K. Aonash, S.Shige, and K. Okamoto, 2006: Development of over-ocean SSM/I rain retrieval algorithm in the GSMaP project. *Proc. of IGARSS 2006*, 2588-2591.

Hou, A. Y., R. K. Kakar, S. Neeck, A. A. Azarbarzin, C. D. Kummerow, M. Kojima, R. Oki, K. Nakamura, and T. Iguchi, 2014: The global precipitation measurement mission. *Bull. Amer. Meteor. Soc.*, 95, 701-722.

Kachi, M., T. Kubota, T. Ushio, S. Shige, S. Kida, K. Aonashi, and K. Okamoto, 2011: Development and utilization of "JAXA Global Rainfall Watch" system. *IEEJ Transactions on Fundamentals and Materials*, 131, 729-737. (In Japanese with English abstract)

Kida, S., S. Shige, T. Kubota, K. Aonashi, and K. Okamoto, 2009: Improvement of rain/no-rain classification methods for microwave radiometer observations over ocean using the 37-GHz emission signature. *J. Meteor. Soc. Japan*, 87A, 165-181.

Kida, S., S. Shige, T. Manabe, T. S. L'Ecuyer, and G. Liu, 2010a: Cloud liquid water path for the rain/no-rain classification method over ocean in the GSMaP algorithm, Trans. *JSASS Aerospace Tech. Japan*, 8, No. ists27, Pn_19-Pn_23.

Kida, S., S. Shige, and T. Manabe, 2010b: Comparison of rain fractions over tropical and sub-tropical ocean obtained from precipitation retrieval algorithms for microwave sounders. *J. Geophys. Res.*, 115, D24101, doi:10.1029/2010JD014279.

Kida, S., T. Kubota, S. Shige, and T. Mega, 2017: Development of a Rain/No-Rain Classification Method over Land for the Microwave Sounder Algorithm, *Remote Sensing of Aerosols, Clouds, and Precipitation*, Chapter 12, 249-265.

Kirstetter, P.-E., and Coauthors, 2012: Toward a framework for systematic error modeling of spaceborne precipitation radar with NOAA/NSSL ground radar–based National Mosaic QPE. *J. Hydrometeor.*, 13, 1285–1300.

Kobayashi, S., Y. Ota, Y. Harada, A. Ebita, M. Moriya, H. Onoda, K. Onogi, H. Kamahori, C. Kobayashi, H. Endo, K. Miyaoka, and K. Takahashi, 2015: The JRA-55 Reanalysis: General specifications and basic characteristics. *J. Meteor. Soc. Japan*, 93, 5-48.

Kozu, T, T. Kawanishi, H. Kuroiwa, M. Kojima, K. Oikawa, H. Kumagai, K. Okamoto, M. Okumura, H. Nakatshka, and K. Nishikawa, 2001: development of precipitation radar onboard the Tropical Rainfall Measuring Mission (TRMM) satellite. *IEEE Trans. Geosci. Remote Sens.*, 39, 102-116.

Kubota, T., S. Shige, H. Hashizume, K. Aonashi, N. Takahashi, S. Seto, M. Hirose, Y. N. Takayabu, T. Ushio, K. Nakagawa, K. Iwanami, M. Kachi, and K. Okamoto, 2007: Global precipitation map using satelliteborne microwave radiometers by the GSMaP Project : Production and validation. *IEEE Trans. Geosci. Remote Sens.*, 45, 2259-2275.

Kubota, T., S. Shige, K. Aonashi, K. Okamoto, 2009a: Development of nonuniform beamfilling correction method in rainfall retrievals for passive microwave radiometers over ocean using TRMM observations. *J. Meteor. Soc. Japan*,87A, 153-164.

Kubota, T., T. Ushio, S. Shige, S. Kida, M. Kachi, and K. Okamoto, 2009b: Verification of high resolution satellite-based rainfall estimates around Japan using gauge-calibrated ground radar dataset. *J. Meteor. Soc. Japan*, 87A, 203-222.

Kubota, T., S. Shige, M. Kachi, and K. Aonashi. 2011: Development of SSMIS rain retrieval algorithm in the GSMaP project. *Proc ISTS*, 2011-n-46.

Kubota, T., G. Liu, T. Tashima, and R. Oki, 2018: Development of snowfall estimation method in Global Satellite Mapping of Precipitation (GSMaP) product. *JpGU meeting 2018*, Chiba, Japan, May 2018.

Kummerow, C., W. Barnes, T. Kozu, J. Shiue, and J. Simpson, 1998: The Tropical Rainfall Measuring Mission (TRMM) sensor package, *J. Atmos. Oceanic Technol.*, 15, 808–-816.

Mega, T. and S. Shige, 2016: Improvements of rain/no-rain classification methods for microwave radiometer over coasts by dynamic surface-type classification. *J. Atmos. Oceanic Technol.*, 33, 1257-1270.

Mega, T., T. Ushio, T. Matsuda, T. Kubota, M. Kachi and R. Oki, 2019: Gauge-adjusted Global Satellite Mapping of Precipitation (GSMaP_Gauge), *IEEE Trans. Geosci. Remote Sens.*, in press, doi: 10.1109/TGRS.2018.2870199.

Liu, G., 1998: A fast and accurate model for microwave radiance calculation, *J. Meteor. Soc. Japan*, 76, 335-343.

Liu, G., and E.-K. Seo, 2013: Detecting snowfall over land by satellite high-frequency microwave observations: The lack of scattering signature and a statistical approach. *J. Geophys. Res. Atmos.*, 118, 1376-1387.

Okamoto, K., T. Iguchi, N. Takahashi, K. Iwanami and T. Ushio, 2005: The global satellite mapping of precipitation (GSMaP) project. *Proc. of IGARSS 2005*, 3414-3416.

Otsuka, S., S. Kotsuki, and T. Miyoshi, 2016: Nowcasting with data assimilation: A case of global satellite mapping of precipitation. *Wea. Forecasting*, 31, 1409-1416.

Petty, G. W., 1994: Physical retrievals of over-ocean rain rate from multichannel microwave imagery. Part I: Theoretical characteristics of normalized polarization and scattering indices. *Meteorol. Atmos. Phys*, 54, 79-99.

Scofield, R. A., and R. J. Kuligowski, 2003: Status and outlook of operational satellite precipitation algorithms for extreme-precipitation events. *Wea. Forecasting*, 18, 1037-1051.

Seto, S., N. Takahashi, T. Iguchi, 2005: Rain/no-rain classification methods for microwave radiometer observations over land using statistical information for brightness temperatures under no-rain conditions. *J. Appl. Meteor.*, 44, 1243-1259.

Seto, S., T. Kubota, N. Takahashi, T. Iguchi, T. Oki, 2008: Advanced rain/no-rain classification methods for microwave radiometer observations over land. *J. Appl. Meteo. Clim.*, 47, 3016-3029.

Seto, S., T. Kubota, and S. Shige, 2016: Production of the rain/no-rain classification database for GPM microwave radiometer observations over land. *MSJ spring meeting 2016*, D405, Tokyo, Japan, May 2016 (in Japanese).

Shige, S., T. Yamamoto, T. Tsukiyama, S. Kida, H. Ashiwake, T. Kubota, S. Seto, K. Aonashi and K. Okamoto, 2009: The GSMaP precipitation retrieval algorithm for microwave sounders. Part I: Over-ocean algorithm. *IEEE Trans. Geosci. Remote Sens*, 47, 3084-3097.

Shige, S., S. Kida, H. Ashiwake, T. Kubota, and K. Aonashi, 2013: Improvement of TMI rain retrievals in mountainous areas. *J. Appl. Meteor. Climatol.*, 52, 242-254.

Shige, S., M. K. Yamamoto, and A. Taniguchi, 2014: Improvement of TMI rain retrieval over the Indian subcontinent. *remote sensing of the terrestrial water cycle*, geophysical monograph 206, Edited by V. Lakshmi, American Geophysical Union, 27-42.

Sims, E.M. and G. Liu, 2015: A Parameterization of the Probability of Snow–Rain Transition. *J. Hydrometeor.*, 16, 1466-1477.

Smith, E. A., J. E. Lamm, R. F. Adler, J. Alishouse, and K. Aonashi, E. Barrett, P. Bauer, W. Berg, A. Chang, R. Ferraro, J. Ferriday, S. Goodman, N. Grody, C. Kidd, D. Kniveton, C. Kummerow, G. Liu, F. Marzano, A. Mugnai, W. Olson, G. Petty, A. Shibata, R. Spencer, F. Wentz, T. Wilheit, and E. Zipser, 1998: Results of the WetNet PIP-2 project. *J. Atmos. Sci.*, 55, 1483–1536.

Skofronick-Jackson, G., W.A. Petersen, W. Berg, C. Kidd, E.F. Stocker, D.B. Kirschbaum, R. Kakar, S.A. Braun, G.J. Huffman, T. Iguchi, P.E. Kirstetter, C. Kummerow, R. Meneghini, R. Oki, W.S. Olson, Y.N. Takayabu, K. Furukawa, and T. Wilheit, 2017: The Global Precipitation Measurement (GPM) Mission for Science and Society. Bull. Amer. Meteor. Soc., 98, 1679–1695.

Takahashi, N., and J. Awaka, 2007: Introduction of a melting layer model to a rain retrieval algorithm for microwave radiometers. *Proc. 25th IGARSS*, 3404-3409.

Takayabu, Y. N., 2008: Observing Rainfall Regimes Using TRMM PR and LIS Data. *GEWEX Newsletter*, 18, 9-10.

Tan, J., W.A. Petersen, and A. Tokay, 2016: A Novel Approach to Identify Sources of Errors in IMERG for GPM Ground Validation. *J. Hydrometeor.*, 17, 2477–2491.

Taniguchi, A., S. Shige, M. K. Yamamoto, T. Mega, S. Kida, T. Kubota, M. Kachi, T. Ushio, and K. Aonashi, 2013: Improvement of high-resolution satellite rainfall product for Typhoon Morakot (2009) over Taiwan. *J. Hydrometeor.*, 14, 1859-1871.

Ushio, T., T. Kubota, S. Shige, K. Okamoto, K. Aonashi, T. Inoue, N., Takahashi, T. Iguchi, M. Kachi, R. Oki, T. Morimoto, and Z. Kawasaki, 2009: A Kalman filter approach to the Global Satellite Mapping of Precipitation (GSMaP) from combined passive microwave and infrared radiometric data. *J. Meteor. Soc. Japan*, 87A, 137-151.

Vicente, G. A., R. A. Scofield, and W. P. Menzel, 1998: The operational GOES infrared rainfall estimation technique. *Bull. Amer. Meteor. Soc.*, 79, 1883-1898.

Vicente, J. C. Davenport, and R. A. Scofield, 2002: The role of orographic and parallax corrections on real time high resolution satellite erainfall rate distribution. *Int. J.Remote Sens.*, 23, 221-230.

Yamaji, M., T. Kubota, A. Hamada, Y., N. Takayabu, M. Kachi, and K. Aonashi. 2017: Drop Size Distribution observed by Dual-frequency Precipitation Radar onboard Global Precipitation Measurement core satellite. *Proc. ISTS 2017*, 2017-n-17.

Yamamoto, M. K. and S. Shige, 2015: Implementation of an orographic/nonorographic rainfall classification scheme in the GSMaP algorithm for microwave radiometers. *Atmos. Res.*, 163, 36-47.

Yamamoto, M. K., S. Shige, C.-K. Yu, and L.-W. Cheng, 2017: Further improvement of the heavy orographic rainfall retrievals in the GSMaP algorithm for microwave radiometers. *J. Appl. Meteor. Climatol.*, 56, 2607-2619.

Zhang, J., K. Howard, C. Langston, S. Vasiloff, B. Kaney, A. Arthur, S. Van Cooten, K. Kelleher, D. Kitzmiller, F. Ding, D. Seo, E. Wells, and C. Dempsey, 2011: National mosaic and multi-sensor QPE (NMQ) system: Description, results, and future plans. *Bull. Amer. Meteor. Soc.*, 92, 1321–1338.

Zhang, J., K. Howard, C. Langston, B. Kaney, Y. Qi, L. Tang, H. Grams, Y. Wang, S. Cocks, S. Martinaitis, A. Arthur, K. Cooper, J. Brogden, and D. Kitzmiller, 2016: Multi-radar multi-sensor (MRMS) quantitative precipitation estimation: Initial operating capabilities. *Bull. Amer. Meteor. Soc.*, 97, 621-638.